Journal of
Materials Chemistry C

Materials for optical, magnetic and electronic devices

Accepted Manuscript

This article can be cited before page numbers have been issued, to do this please use: S. Zhan, X. Fan, J. Zhang, J. Yang, S. Y. BANG, S. D. Han, D. Shin, S. Lee, H. W. Choi, X. Wang, B. Hou, L. G. Occhipinti and J. M. Kim, *J. Mater. Chem. C*, 2020, DOI: 10.1039/D0TC03838E.

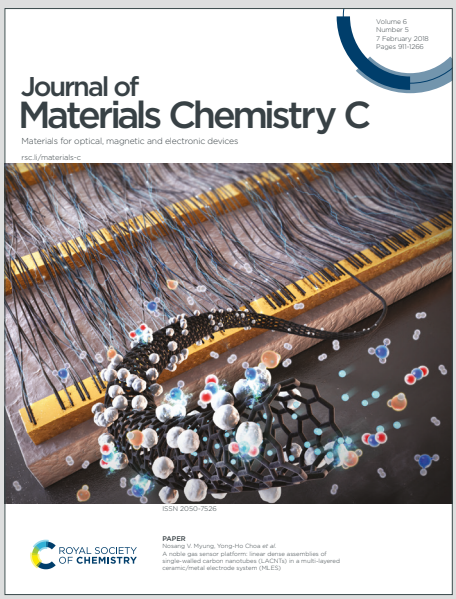

ROYAL SOCIETY OF CHEMISTRY

rsc.li/materials-c

View Article Online
DOI: 10.1039/D0TC03838E

Lattice Marginal Reconstruction Enabled High Ambient-Tolerance Perovskite Quantum Dots Phototransistors

Shijie Zhan,[a] Xiangbin Fan,[a] Jiangbin Zhang,[b,c] Jiajie Yang,[a] Sang Yun Bang,[a] Soo Deok Han,[a] Dong-Wook Shin,[a] Sanghyo Lee,[a] Hyung Woo Choi,[a] Xiaozhi Wang,[d] Bo Hou,[*a,e] Luigi G. Occhipinti,[*a] and Jong Min Kim,[a]

[a] *Electrical Engineering, Department of Engineering, University of Cambridge, Cambridge, CB3 0FA, UK*
E-mail: lgo23@cam.ac.uk
[b] *Cavendish Laboratory, Department of Physics, University of Cambridge, Cambridge CB3 0FA, UK*
[c] *College of Advanced Interdisciplinary Studies, National University of Defense Technology, Changsha 410073, P. R. China.*
[d] *College of Information Science and Electronic Engineering, Zhejiang University, Hangzhou, 310058, China*
[e] *School of Physics and Astronomy, Cardiff University, Cardiff, CF24 3AA, Wales, UK*
E-mail: HouB6@cardiff.ac.uk

Abstract

Perovskite quantum dots (PeQDs) have been developed rapidly as photoactive materials in hybrid phototransistors because of their strong light absorption, broad bandgap customizability, and defect-tolerance in charge-transport properties. The solvent treatment has been well recognized as a practical approach for improving the charge transport of PeQDs and the photoresponsivity of PeQD phototransistors. However, there is a lack of fundamental understanding of the origin of its impacts on the material's ambient stability as well as phototransistor's operational lifetime. Especially, the relationship between surface ligands dissociation and their microstructural reconstruction has not been fully elucidated so far. Herein, we report that a simultaneous enhancement of photoresponsivity and ambient tolerance for PeQD-based hybrid phototransistors can be realized via medium-polarity-solvent treatment on solid-state PeQDs. Our comprehensive optoelectronic characterization and electron microscopic study reveals that the crystal morphology, instead of surface ligands, is the dominating factor that results in the PeQD's stability enhancement associated with the preservation of optical property and quantum confinement. Besides, we unveil a marginal reconstruction process occurred during solvent treatment, which opens up a new route for facets-oriented attachment of PeQDs along the <220> zone axis to suppress the damage from water molecules penetration. Our study yields a new understanding of the solvent impact on PeQD microstructures reconstruction and suggests new routes for perovskite materials and corresponding device operational stability enhancement.

Keywords: Perovskite Quantum Dot, Morphology Transition, Hybrid Phototransistor, Stability, Electron Microscopy

1. Introduction

Inorganic perovskite quantum dots (PeQDs), especially the caesium lead halide ($CsPbX_3$, X = Cl, Br, I) quantum dots hold great potential in perovskite light-emitting diodes, solar cells, and photodetectors, benefitting from their narrow emission line widths, broad bandgap customizability, high defect tolerance, high photoluminescence quantum yield (PLQY) and strong light absorption.[1-8] Recently, PeQD-sensitized hybrid phototransistors attract considerable interest in the broadband photodetection because of their higher photoresponsivity in a broader range of wavelengths than conventional photodetectors based on silicon and indium gallium arsenide.[9, 10] Moreover, these three-terminal active device structure is suitable for integrated-circuit applications, such as image sensors, optical communications, and others.[11-15]

Usually, in order to achieve PeQDs-sensitized phototransistors with excellent performance, a strong carrier coupling between adjacent PeQDs need to be accomplished. Generally, it is realized by removing aliphatic surface ligands such as oleic acid (OA) and oleylamine (OAm).[16, 17] Solvent washing has been widely adapted to remove bulky ligands on PeQDs due to its processing simplicity, as well as its effectiveness in reaching a tightly packed structure.[18-20] For instance, it has been reported that polar solvent washing could trigger the self-assembly of PeQD.[18, 19] Such polar solvent-induced PeQD self-assembly can generate a band-like carrier transport, but can also bring irreversible structural damage during dissociation and protonation of surface ligands.[2] To avoid undesired damage during a polar solvent washing process and to achieve robust stability of PeQDs, a variety of solvents with low or medium polarity have been proposed, such as esters, alcohols, γ-butyrolactone and acetonitrile.[20-23] However, most of the published reports employing the medium-polarity solvent approach do not provide sufficient information about the ambient stability of treated PeQDs, neither about the lifetime of solvent-treated devices, leaving this vital aspect of device stability mostly uncovered in literature. Even though the solvent treatment can achieve densely coupled PeQDs, there is also a strong potential in materials and devices stability degradation, which will pose limitations to device design, fabrication, and operation. Nevertheless, there is a lack of fundamental understanding of the origin of solvent impacts on the material's ambient stability as well as phototransistor's operational lifetime. Especially, the relationship between surface ligands dissociation and their microstructural reconstruction has not been fully

View Article Online
DOI: 10.1039/D0TC03838E

elucidated so far. In order to address this issue, it is crucial to understand the fundamental processes occurring at the initial stage during the medium-polarity-solvent interaction with solid-state PeQDs, such as microscopic lattice structure, morphology and resultant device figure of merit variation as a function of time and external bias.

In this study, we conducted a medium-polarity-solvent treatment on solid-state PeQDs to demonstrate blue inorganic PeQD ($CsPbBr_3$) hybrid phototransistors with both enhanced photoresponsivity and ambient tolerance and then explored the microscopic mechanism underlying the improvement. Firstly, we proved that the medium-polarity-solvent washing could boost the photoresponsivity of PeQD/indium-gallium-zinc-oxide (InGaZnO) hybrid phototransistors up to 3 orders of magnitude. Then, electron microscopy studies and optical measurements showed that treated PeQDs coupled with each other associated with detached surface ligands and changed surface morphology. Also, we confirmed that solvent treatment-induced oriented-attachment do not have a significant impact on the optical properties and quantum confinement of PeQDs. After the disassociation of ligands, ethyl acetate (AcOEt)-treated PeQDs exhibited superior stability in the ambient atmosphere compared with the untreated film, which results in the excellent ambient tolerance of PeQD-based hybrid phototransistors-with a 1/e lifetime of over 360 hours. In order to elucidate the PeQD stability enhancement after ligands dissociation, we conducted further electron microscopy studies, and we observed that an AcOEt-induced solid-state marginal reconstruction process occurred associated with PeQD surface morphology variation and facet assembly. More importantly, we found the crystal morphology, instead of surface ligands, is the dominating factor that results in the PeQD and phototransistor stability enhancement. This work demonstrates and explains the effect of medium-polarity solvent in simultaneously achieving high photoresponsivity and high ambient stability for PeQD hybrid phototransistors, which provides new insights for future perovskite materials and optoelectronic devices stability studies.

2. Experimental details

Blue colour emission PeQDs are well-known challenge materials in perovskite optoelectronic device efficiency and stability compared with green and red ones.[2, 24] This work, therefore, focused on blue $CsPbBr_3$ PeQDs to obtain a fundamental understanding of the origin of solvent impacts on the material's ambient stability as

View Article Online
DOI: 10.1039/D0TC03838E

well as phototransistor's operational lifetime.[25, 26] The blue PeQDs were synthesized according to a previously reported work with a slight modification (see Perovskite Quantum Dot Synthesis in Supporting Information).[27] Fig. S1 shows the blue emission of the as-synthesized PeQD solution in octane. Hybrid blue PeQDs phototransistors were fabricated by depositing as-synthesized PeQDs onto the thin film transistors (TFTs) with InGaZnO channels, where the TFTs were made according to the method used in our previous work (see Device Fabrication in Supporting Information).[28] The transfer curve of a typical InGaZnO TFT along with its figure of merit performance is shown in Fig. S2. To form a clean interface between PeQDs and oxide channels, InGaZnO TFTs was thoroughly washed with AcOEt and baked at 100 ^{o}C before PeQD deposition. A drop of 15 mg/ml PeQD solution in octane was spun coated onto the oxide channel at 2000 rpm for 45 s and then annealed at 80 ^{o}C in an N_2 environment. The PeQD film covering the contact parts for source, drain and gate electrodes was wiped in the end to have good contact during measurement. No encapsulation process was done for all devices. Finally, a solvent washing process was conducted on the PeQD film that was deposited on the transistor channel to detach the aliphatic ligands by adopting AcOEt, a universal medium-polarity solvent. Fig.1a shows the illustration of the solid-state solvent treatment process adopted in this work. Ethyl acetate (99.8 %) was dropped onto the film and stayed for 40 s to remove OA and OAm ligands at surface, followed by spinning to dry out the solvent at 2000 rpm for 30 s. Afterwards, the device was annealed at 100 ^{o}C for 10 min in the glove box. Here AcOEt was employed since it was proved to be one of the effective solvents for purifying and recovering PeQDs from raw reaction solution during synthesis.[21, 29] The details of material and device characterization are included in Supporting Information.

3. Results and discussion

3.1 Medium-Polarity-Solvent-Induced Charge Transport Enhancement of PeQDs

The device structure is demonstrated through a high-angle annular dark-field imaging scanning transmission electron microscopy (HAADF-STEM) cross-section analysis (Fig. 1b) that displays the stacking sequence of the device, Si/SiO_2/InGaZnO/Al/PeQDs, with InGaZnO (45 nm) as the channel layer, Al (100 nm) as the drain/source electrode and PeQDs (85 nm) as the photoactive layer. The composition of PeQDs was confirmed by the HAADF-STEM electron dispersive X-ray (EDX) elemental mapping (Fig. 1b)

View Article Online
DOI: 10.1039/D0TC03838E

and the profile elemental line-scan (Fig. S3). It could be seen that the PeQDs consist of Cs, Pb, and Br with a proper stoichiometric composition ratio of 1:1:3. It is worth noting that different anion coupled PeQDs could exhibit distinct optoelectronic properties. For the sake of consistency, Br was the only anion implemented during our synthesis.[29, 30] Before studying the stability of the PeQDs during solvent washing, we first investigated the photoresponsivity of the PeQD hybrid phototransistors after solvent treatment to verify that AcOEt washing could promote PeQD's charge transport. The measurement was conducted under a 475 nm wavelength light excitation with a power density of 7.73 $\mu W/cm^2$. Fig. 1b exhibits a good photoresponsivity improvement of the hybrid phototransistor after AcOEt treatment with up to ~1400 times enhancement (V_{DS} = 5 V, V_{DS}: drain-source voltage). The AcOEt-treated phototransistor exhibited the highest photoresponsivity of 5.4×10^4 A/W while the untreated phototransistor had a maximum photoresponsivity of 6.8×10^3 A/W (see Photoresponsivity Calculation in Supporting Information). Furthermore, a comparison of photoresponsivity at V_{DS} = 15 V presents almost the same ratio of the enhancement (Fig. S4). Such a remarkable boost is mainly attributed to a higher density of excited electrons injected from the photoactive layer into the channel layer, which indicates an improved charge transport in the PeQD layer during AcOEt washing.

To have a more in-depth understanding of the effect of the AcOEt treatment on the hybrid phototransistors, we further carried out the two-dimensional (2D) photoresponsivity mappings analysis as a function of the gate and drain voltage (Fig. 1d and 1e). Similar distribution patterns of the photoresponsivity appear in both mappings with high photoresponsivity around V_{DS} = 5 V and V_{GS} = 2.5 V (V_{GS}: gate-source voltage), where the AcOEt-treated phototransistor possesses much higher photoresponsivity throughout different drain and gate bias (the responsivity scale of Fig. 1e is five times higher than that of Fig. 1d). In both mappings figures, the photoresponsivity increases with the rise of V_{DS} or V_{GS} before reaching the peak value. Within a proper range, the increase of V_{GS} in the positive range attracts more electrons injecting from the PeQD layer to the InGaZnO channel. Under a higher V_{DS} bias, injected electrons generate higher drain currents. However, the photoresponsivity of both untreated and treated PeQD phototransistors decreases with a further rise of bias. This is due to the higher probability of scattering and recombination with excessive carrier density.[31]

View Article Online
DOI: 10.1039/D0TC03838E

In addition to the enhanced photoresponsivity, the photosensitivity (drain current under light/drain current without light) of the AcOEt-treated phototransistor also exhibited a significant enhancement (Fig. 1f). The photosensitivity of both untreated and treated phototransistors peaked at 3.8×10^2 and 1.1×10^5, respectively. The photosensitivity along various power density was further measured for the AcOEt-treated sample, showing enhanced photosensitivity with increasing laser irradiation power (Fig. S5). While the photoresponsivity of the AcOEt-treated phototransistor reaches its peak with gate voltage ~2.5 V, its photosensitivity has different voltage-dependent distribution with the maximum at -10.5 V due to the low dark current. Such a difference distribution suggests a trade-off between photoresponsivity and photosensitivity, where an optimal compromise point between them could be reached by adequate selection of a gate voltage. Under different power density, the photosensitivity increases from around 10^2 at 0.05 $\mu W/cm^2$ to over 10^5 at 48.75 $\mu W/cm^2$, with the peak position of gate bias almost unchanged. The transfer curve at a different power density of incident light also shows an increasing photocurrent/dark current ratio with the rise of power density (Fig. S6). Fig. S7a and S7b present the power response of the photocurrent and photoresponsivity for the AcOEt-treated PeQD phototransistor. The photocurrent as a function of power density was fitted with a power-law equation ($y = bx^a$) before saturation, where a = 0.505 was obtained. Such a low power index of 0.505 indicates the existence of trap states at surfaces of PeQDs and the interface between PeQDs and the InGaZnO channel.[31] Therefore, photoresponsivity has a decreasing trend with the rise of power density, especially after the photocurrent gets saturated. The multi-exponential decay of time-resolved PL (Fig. S7c) for both untreated and treated PeQD thin films proves the presence of trap states, consistent with the results in the power response mentioned above.[32] Apart from the response under the incident light at 475 nm, the AcOEt treated hybrid phototransistor has a better characteristic wavelength dependency with the peak responsivity featuring at ~475 nm (Fig. S8). To compare this PeQD hybrid phototransistor with previous works, Table. S2 summarizes performance of PeQD hybrid phototransistors developed in recent studies.

To understand the fundamental physicochemical mechanism behind the enhanced photoresponsivity, we performed Fourier-transform infrared spectroscopy (FTIR) and electron microscopy characterization systematically on solvent-treated PeQDs. FTIR transmission spectrum proves the detachment of OA/OAm ligands with the evidence

View Article Online
DOI: 10.1039/D0TC03838E

of the reduction of CH_2 peaks around 2850 cm^{-1} and 2920 cm^{-1} (Fig. 2a).[33] Quantitative comparison of the vibration peaks tells that a considerable amount of the aliphatic ligands were removed during the solid-state solvent washing. Fig. 2b illustrates the schematics of charge transport among PeQDs before and after AcOEt washing. With less passivated surfaces, the PeQDs tend to couple with each other and form pathways for better charge transport.[18, 19]

Microscopic images further verify the solvent-induced PeQD coupling and attachment. Fig. 2c and 2d exhibit TEM analysis result of the PeQDs before and after the AcOEt treatment, which show the diameter of as-prepared PeQDs are around 15 nm. As shown in Fig. 2c and the inset image, pristine PeQDs exhibit cubic shapes and are well separated from each other by bulky OA/OAm ligands. Additional TEM and HAADF-STEM images of untreated PeQDs taken in a different area are shown in Fig. S9a, and Fig. S9b. After AcOEt washing, the PeQDs turned to pack together due to the removal of surface passivation with a significant reduction in the dot-to-dot distance, as shown in Fig. 2d.

The inset image of Fig. 2d presents the overview of densely packed PeQD film (200 nm scale bar). Fig. 2e gives a high-resolution HAADF-STEM image of the solvent (50 nm scale bar), which exhibit the morphology of PeQD. Compared with the STEM image of the untreated PeQDs (Fig. S9c), the higher resolution of Fig. 2e, in some degree, implies the removal of most surface ligands. The additional HAADF-STEM images of the treated PeQDs in Fig. S9d~S9f, providing further evidence about the evolution of PeQDs ensemble during the solvent treatment. Under a tightly packed configuration, a strong wavefunction coupling can be established between adjacent PeQDs which facilitate electron transport in PeQD solid films. Therefore, more electrons can be injected into the InGaZnO channel, which is energetically more efficient than pristine PeQD ensembles that insulating ligands block most electron transport before reaching the PeQD/InGaZnO interface. The statistical ratio of the rectangle and truncated nanocrystal morphology was shown in Fig.2f according to PeQDs' shape distribution in TEM/STEM images (see Statistical Ratio Counting in Supporting Information), which indicate there is morphology transition after AcOEt treatment (highlighted in Fig. 2c and 2d). This will be further discussed in the following sections.

View Article Online
DOI: 10.1039/D0TC03838E

To understand the origin of the high photoresponsivity, we need to find out the evolution of the PeQD optical properties during the solvent treatment. As shown in Fig. 2g, the solvent treated-PeQD film well retained the original optical property with only a slightly intensity change in both stationary PL and absorption spectra. Indeed, unlike conventional inorganic quantum dots, PeQDs provide high quantum confinement irrespective of the crystal size or morphology, because of their intrinsic structure is similar to multiple quantum wells.[34-36] The slight reduction in the PL and absorption intensity could be attributed to the stronger coupling of carrier wavefunction in PeQDs. It is noticed that the PL spectra have a much smaller reduction and red-shift compared with the absorption spectra which indicate there is a negligible amount of defect states which related to non-radiative recombination. It indicates the maintenance of quantum confinement in PeQDs with inherent excitonic features that enable high photoresponsivity from as-prepared phototransistors. However, it remains a doubt whether the AcOEt-washed PeQDs become vulnerable in ambient conditions with a less passivated surface and changed morphology. Considering the crucial role of PeQD's stability in phototransistors, the impact of AcOEt treatment on PeQDs' ambient durability was further studied, which will be presented in the following paragraph.

3.2 Medium-Polarity-Solvent-Induced Stability Enhancement of PeQDs

To explore the stability of PeQD films, we measured the PL spectra for both pristine and solvent-treated PeQD films after 2640-hour-storage in the ambient condition without light. Fig. 3a shows that the untreated film after storage suffered a more severe PL reduction than the treated sample (Fig. 2e) given the fact that the pristine untreated PeQD film possessed a higher PL intensity than the treated one. Moreover, the full width at half maximum (FWHM) of the pristine PeQD film broadened a lot (from ~27.4 nm to 32 nm) after ambient storage for 2640 hours while the FWHM of the AcOEt-treated sample well maintained at ~27.5 nm under the same storage condition (Fig. 3b). With solvation and infiltration of water molecules, the structure of PeQDs could be undermined.[37] In addition, the untreated PeQDs suffered from a severe hydration-assisted nanocrystal aggregation and growth.[2] Both of these two degradation mechanism resulted in PL intensity reduction and quantum confinement weakening, which caused the significant broadening in the FWHM of the untreated PeQD film. On the contrary, little change of the treated film's FWHM indicated an enhancement of

View Article Online
DOI: 10.1039/D0TC03838E

PeQD stability during AcOEt treatment, which could be verified by the microscopic study and accounted by a marginal reconstruction process in Section 3.3.

The AcOEt-treated PeQD hybrid phototransistor device lifetime characterization was performed under a benchmark analysis protocol. Typically, to test the stability in the ambient atmosphere, we stored devices in the ambient condition without light (24.8℃ and relative humidity of 40%). The photoresponsivity versus gate voltage measured after a specific period is plotted in Fig. 3c. While a remarkable drop of photoresponsivity was noticed during the first 12 hours, no significant degradation was found between 12 hours and 72 hours as well as between day-10 and day-14. Remarkably, the treated PeQD phototransistor on day-14 still has a much higher photoresponsivity compare to the untreated device on day-1 (dotted line in Fig. 3c), which implies the advantage of AcOEt washing in achieving both high photoresponsivity and robust durability.

Fig. 3d shows the photoresponsivity versus storage time under a drain current of 10 nA, which exhibits a two-phase drop process-a fast decay period before 12 hours and then a slow decay afterwards. Such a two-phase reduction phenomenon could be attributed to different degradation processes: i) as mentioned above, part of ligands remained on the PeQD surface, while some parts of PeQD surfaces were unpassivated after washing; ii) in the meantime, some parts of PeQD surfaces were reconstructed during AcOEt treatment. Therefore, in the first stage, the unpassivated surfaces without reconstruction could degrade in a short time. Afterwards, the remaining parts of surfaces, including the ligand-passivated and reconstructed ones, might undergo a slower degradation process. The details of the reconstruction process, as well as experimental evidence, will be further explained in the following high-resolution HAADF-STEM microscopic discussions.

Exponential decay ($R \sim exp^{-t/\tau}$) was used to fit the second stage photoresponsivity decline, where R, t, τ represent photoresponsivity, time and decay constant, respectively. It shows that the 1/e lifetime of the treated device is ~360 hours, and the phototransistor could maintain photoresponsivity over 1000 A/W after 1000-hour-exposure in the ambient atmosphere. With such a slow decay, the AcOEt-treated PeQD hybrid phototransistor possesses a considerable long lifetime, potentially, could be over months. Besides, the declining process shows a similar trend with a drain current of 10

View Article Online
DOI: 10.1039/D0TC03838E

nA or 10 μA (Fig. S10), indicating that the photoresponsivity variation comes only from the intrinsic degradation of PeQDs.

It is well-considered that water molecule serves as one of the primary reason for PeQD destruction.[2] Therefore, an extreme condition with 80% humidity (RH 80%) at room temperature was adopted to explore the humidity tolerance of as-prepared PeQD phototransistors. It should be noted that RH 80% corresponds to the average relative humidity in tropical areas with frequent precipitation, such as Singapore. Typically, the devices were stored in a box with a controlled humidity level without any light, as illustrated in Fig. S11. Fig. S12a shows the photoresponsivity curve versus drain current measured after a different period. Consistent with the fact that PeQDs degrade when exposed to water, the responsivity dropped much faster compared to the deterioration speed under the condition with RH 40% (Fig. S12b).[2] Nevertheless, even under such an extreme condition, the solvent-treated phototransistor, after half a month (360 hours), could still maintain a responsivity close to the value of the untreated device before degradation (dotted line). Given the condition that all of our PeQD phototransistors are not encapsulated, it is remarkable to have such a PeQD device lifetime and humidity tolerance over half a month.

The robust optical property and ambient stability of ensemble PeQDs indicate that the optoelectronic property of PeQDs, to some degree, mainly depends on the morphology rather than surface ligands. For instance, though the ensemble PeQDs have much closer distanced after removal of a considerable amount of ligands, the PL and absorption spectra still kept most of their intensity. It means the PeQDs well maintain their quantum confinement even most of the surface ligands have been detached. Furthermore, the ensemble PeQD film surprisingly did not lose ambient stability, instead, showing better stability after solvent treatment. All of these results pointed out the significant role of PeQD morphology in modulating PeQD's stability.

3.3 Marginal Reconstruction of PeQDs during AcOEt treatment

To fully elucidate the relationship between the crystal morphology and materials stability, we carried out comprehensive electron microscopy studies on solvent treated PeQD film and as-prepared phototransistors. According to the azimuthally integrated electron beam diffraction (i-ED) and HRTEM results, it can be seen that during the AcOEt washing process, a solvent-assisted marginal reconstruction occurs at the

View Article Online
DOI: 10.1039/D0TC03838E

surface of PeQDs. The i-ED pattern in Fig. 4a implies that multiple facets exist in the untreated PeQDs, including {100}, {111}, {200}, {210} and {300}. This multi-pattern result is consistent with the previously reported nano-twin structures.[38, 39] Despite the complex structure in the PeQD, the facets in the {200} group are exposed at the surface of the untreated PeQD with a cubic morphology (Fig. 4c). After AcOEt washing, the i-ED of treated PeQDs show newly generated {110} and {220} patterns in the reciprocal space. The diffraction result is consistent with the HRTEM image of treated PeQDs, where a new facet group {220} comes up at the PeQD surface (Fig. 4d). This is further supported by the electron diffraction (ED) image of untreated (Fig. S13) and treated PeQDs (Fig. S14) where the ED pattern of treated PeQDs has the sharp crystalline spots on the {220} diffraction ring. From this evidence, it can be concluded that a surface-etching process is taking place during AcOEt washing, where the surfaces of PeQDs were partially converted from single-facets to multi-facets ({220}, {200}) as presented in the schematic of Fig. 4e.

Further electron microscopy studies (Fig. 3) reveals a plausible mechanism of {220} surface evolution through a marginal reconstruction which is occurred right after the surface-etching process. That is, without the passivation of aliphatic ligands at the surface, the $CsPbBr_3$ PeQD with a cubic-phase is thermodynamically erratic at room temperature, which undergoes a morphology transition to initiate oriented attachment of unstable facets of PeQDs to form a more stable ensemble structure.[18] As captured by the HAADF-STEM analysis (Fig. 5), the edge-truncated PeQDs attached with each other in a dense arrangement. We further validated our consumption via in situ EDX mapping (Fig. S15), which confirmed the particles shown in Fig.5 are $CsPbBr_3$ PeQDs. An atomic-structure illustration which highlights the interface between the three attached PeQDs is shown in Fig.5, as well as the HAADF-STEM interface fine features (dotted white circle). According to a previous study, the spacing between QDs linked with ligands of 10 carbons is over 6 nm,[40] thus the average spacing lower than 1 nm (Fig. 5) indicates a close-packed fashion between PeQDs after the removal of surface ligands. Based on the HAADF-STEM image, two sorts of interfaces can be indexed: {200} interface and reconstructed {220} interface. When PeQD surfaces are exposed with facets of the {220} group, water molecules could infiltrate to interact with unpassivated Cs atoms and result in the structural deconstruction. It can be inferred from the HAADF-STEM image that the presence of voids among PeQDs leaves

View Article Online
DOI: 10.1039/D0TC03838E

pathways for water molecules to interact with {220} facets. However, the direct attachment of {220}facets will facilate the coordination between Cs and Br, which can help the 're-passivation' of the vulnerable surfaces against the water penetration. Therefore, based on the stable facets in {200} and assembled facets in the {220} group, the solvent treated PeQDs realise a stable optical and electrical properties in the ambient condition.

4. Conclusion

In conclusion, we illustrate the fundamental mechanisms of the origin of solvent impacts on the PeQD material's ambient stability as well as phototransistor's operational lifetime. More importantly, we uncover a crystal marginal reconstruction process of PeQDs during solvent treatment via using AcOEt, a commonly selected medium-polarity solvent. By efficiently detaching the insulating ligands on PeQDs, the photoresponsivity of the solvent-treated hybrid phototransistor shown up to 1400 times enhancement, achieving over 5.4×10^4 A/W as the maximum while the highest photosensitivity reached over 10^5. The HAADF-STEM analysis directly observed the solvent-induced PeQD-coupling, which not only enhanced the charge transport but also preserved the quantum confinement. Apart from the solvent-induced charge transport enhancement, the stability of PeQD films also shown considerable improvement after AcOEt washing. Stored in the ambient atmosphere with a humidity level of 40% for 2640 hours, the treated PeQD film maintain a much narrower PL FWHM compared to the pristine one. As a result, AcOEt-treated PeQD hybrid phototransistors obtain a 1/e lifetime of 360 hours and maintain over 10^3 A/W after 1000 hours. A morphology transition from cubic shape to edge-truncated was captured in the HRTEM and HAADF-STEM analysis. Based on the ED and HRTEM analysis, we found that the {200} group dominated the surface of the untreated PeQDs. At the same time, the edge-truncated PeQDs have newly generated facets in the {220} group. Though facets in {220} tend to have low moisture resistance, a {220} orientated attachment occurred during AcOEt washing, which prevents water penetration and enhances the stability of PeQD films. Our study yields a new breed of explanation for the role of AcOEt as a medium-polarity solvent to achieve tightly coupled PeQD film with improved stability and robust phototransistor durability. Moreover, our work reveals the critical role of morphology in PeQDs concerning their optical-electrical property and stability, and

View Article Online
DOI: 10.1039/D0TC03838E

introduce a new pathway of perovskite stability enhancement via surface morphology engineering other than commonly adopted ligand chemistry.

Supporting information

See supplementary material for detailed experimental procedures and supporting images.

Author contributions

S.Z. and B.H. conducted the experiments, collected and interpreted the data, and wrote the manuscript. X.F., J.Z., J.Y., S.B., S.D.H., D.W.S., S.L., H.W.C. interpreted the data and revised the manuscript. L.G.O. and J.M.K. guided the work, provided research infrastructure support and revised the manuscript.

Conflicts of interest

There are no conflicts to declare.

Acknowledgements

The authors acknowledge the support from the European Union under the H2020 project 1D-NEON (Grant Agreement No. 685758), and from the Engineering and Physical Sciences Research Council (EPSRC) in the UK under the project SmartQD (EP/P027628/1). We specially acknowledge the discussion and support Felix C. Mocanu provided.

View Article Online
DOI: 10.1039/D0TC03838E

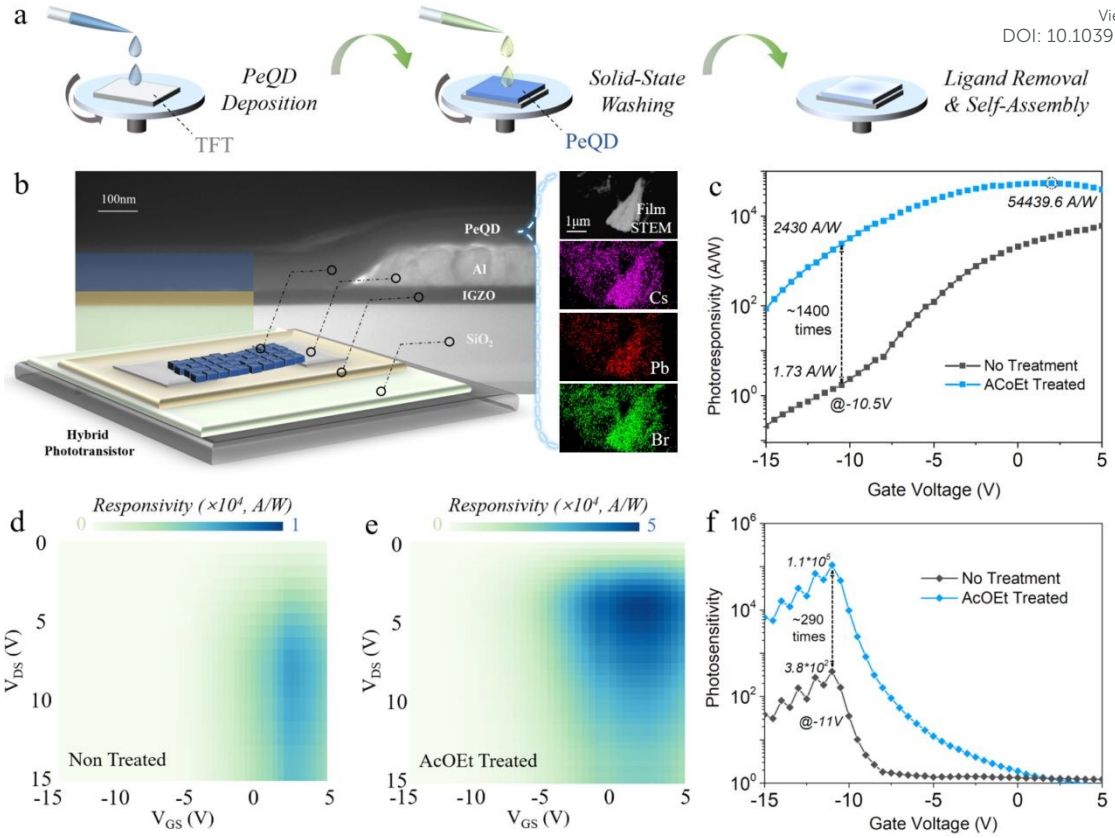

Fig. 1 The phototransistor diagram and characterization. (a) Solid-state washing process illustration for the PeQD washing process. (b) Diagram of the PeQD hybrid phototransistor with InGaZnO as the channel layer and PeQDs as the photoactive layer. The right inset figure shows the STEM image of PeQDs with the EDX mapping for elements, including Cs, Pb, and Br. The cross-section STEM/TEM specimen is prepared by FIB milling. (c) Photoresponsivity of PeQD hybrid phototransistors versus gate voltage before and after AcOEt treatment where V_{DS} = 5 V. (d)(e) Mapping of the photoresponsivity under various gate and drain voltage (d) before and (e) after solvent treatment. The scale bars are placed above both mappings with different maximum values. All characterization from (c)~(e) was done with a light wavelength of 475 nm and a power density of 7.73 μW/cm^2. (f) Photosensitivity of the hybrid phototransistor before and after AcOEt treatment (V_{DS} = 15 V).

View Article Online
DOI: 10.1039/D0TC03838E

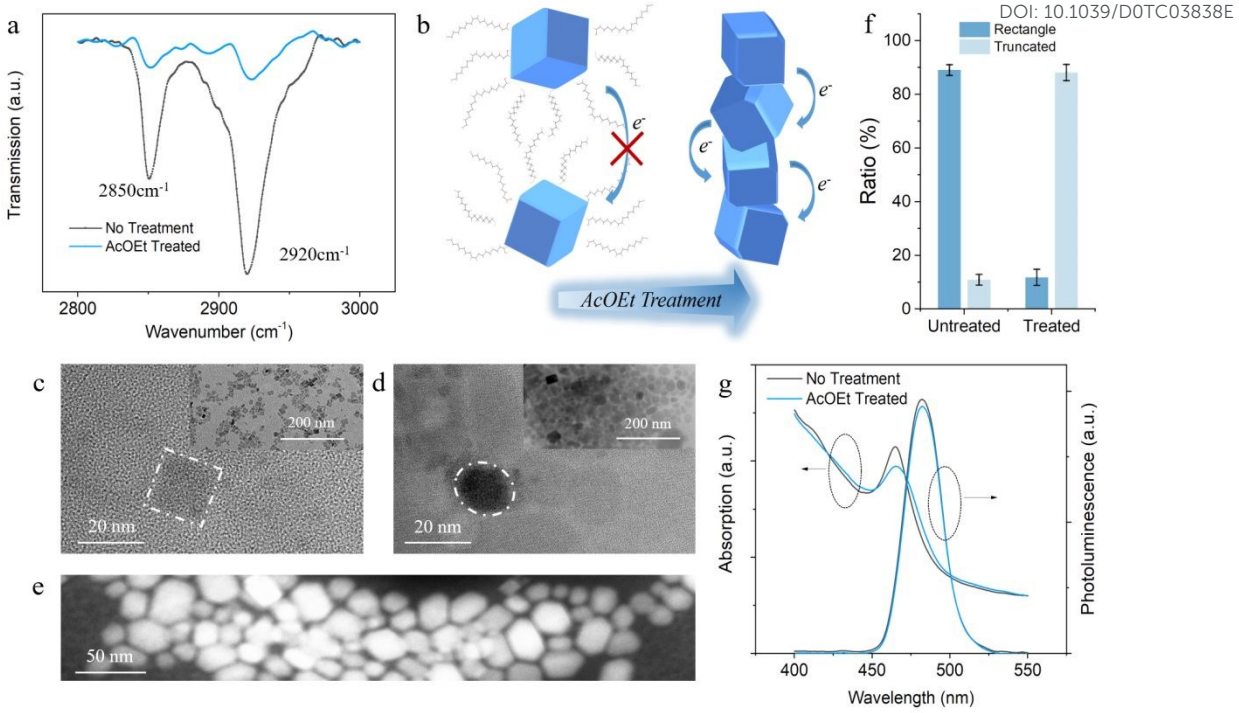

Fig. 2 (a) FTIR transmission spectra within 2800 and 3000 cm^{-1} before (black line) and after (blue line) solvent treatment. (b) Schematics of charge transport improvement induced by AcOEt treatment. (c)(d) TEM images of the PeQDs (c) before and (d) after AcOEt treatment with the scale bar of 20 nm. The inset figures are the TEM images with a scale of 200 nm. (e) The enlarged HAADF-STEM image of solvent-treated PeQDs. (f) The statistical ratio of the rectangle and truncated nanocrystals in untreated and treated PeQDs. (g) The PL and absorption spectra of PeQD films before and after AcOEt treatment.

View Article Online
DOI: 10.1039/D0TC03838E

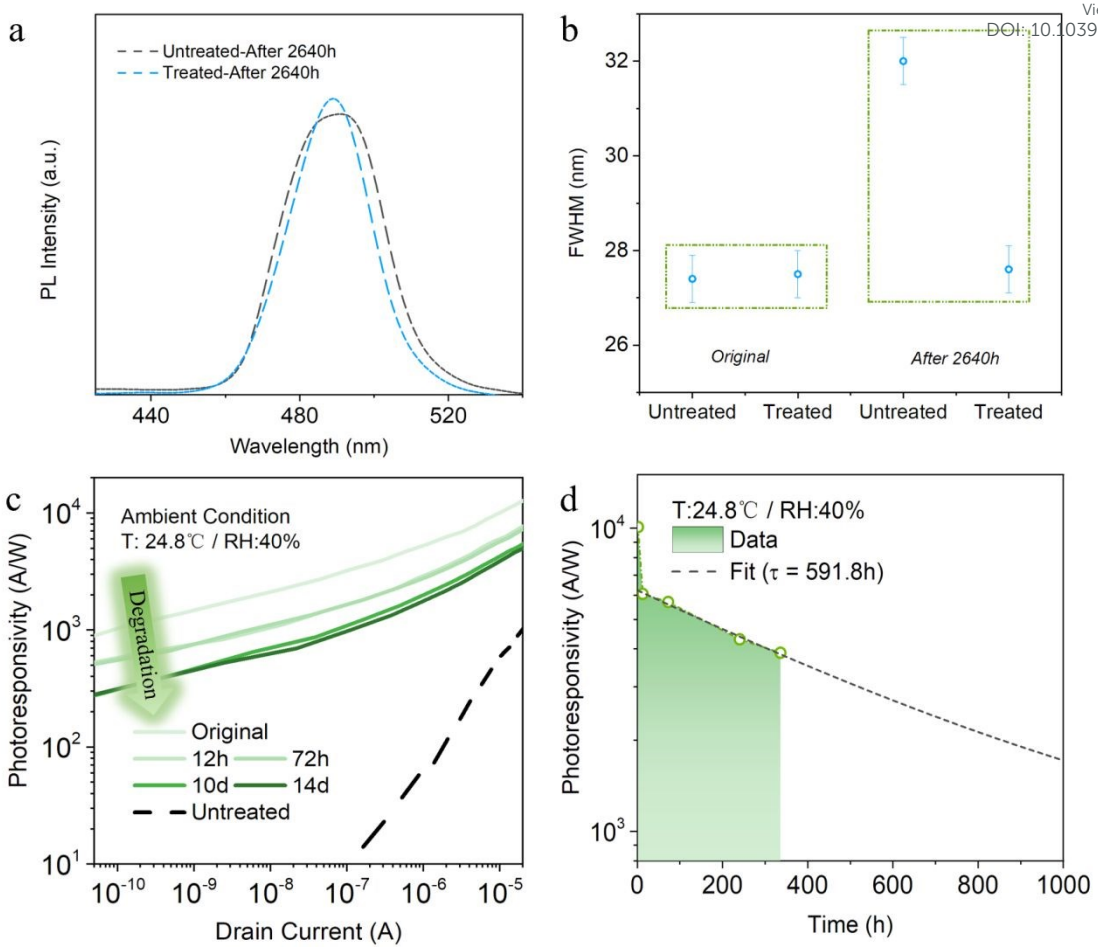

Fig. 3 (a) PL spectra of the untreated and treated PeQD films after ambient exposure for 2640 hours. (b) Comparison of the extracted FHWM for pristine and treated PeQD films before and after storage in the ambient condition for 2640h. The error bar stands for the deviation during measurement and parameter extraction. (c) Photoresponsivity versus drain current of the AcOEt-treated phototransistor before storage (original) and stored for 12 hours, 72 hours, 10 days, and 14 days. (d) Photoresponsivity lifetime analysis of the AcOEt-treated hybrid phototransistor under the ambient condition with a drain current of 10 μA. The black dotted line shows the fitting of the second decay of photoresponsivity.

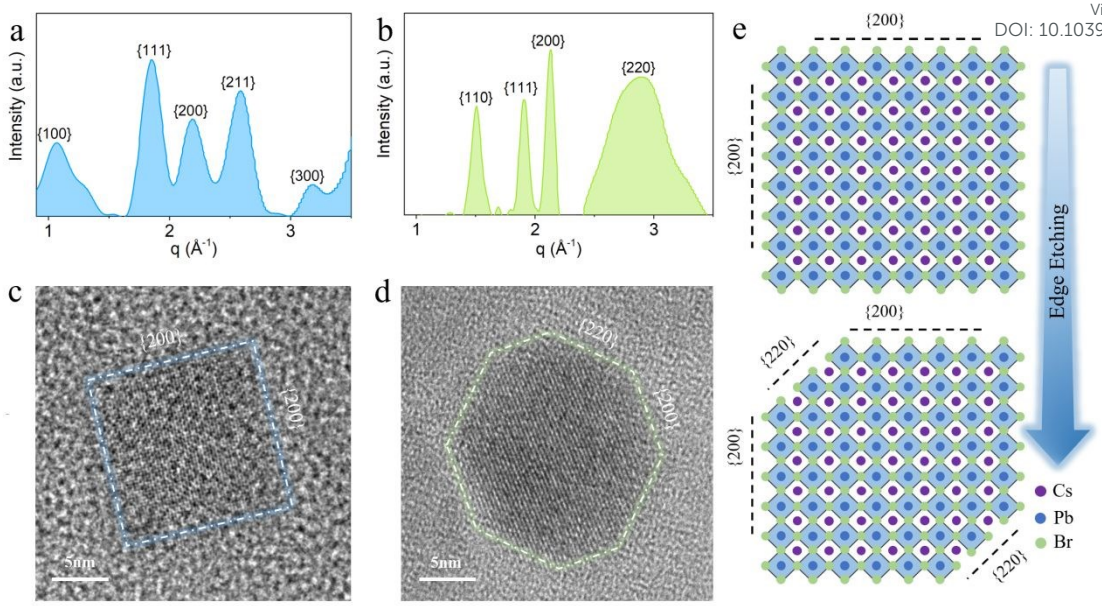

Fig. 4 (a)(b) Azimuthally integrated electron diffraction plot of PeQDs (a) before and (b) after AcOEt treatment. (c)(d) High-resolution TEM images showing different facets on the surface. (c) For the cubic-shaped PeQD before treatment, the {200} facet group was exposed at the surface, (d) while the {220} comes up after the PeQD was edge-truncated. The dotted lines with glow mark the outlines of two PeQD morphology. (e) The schematics of the surface edge-etching process from single-facet to multi-facet during AcOEt treatment.

View Article Online
DOI: 10.1039/D0TC03838E

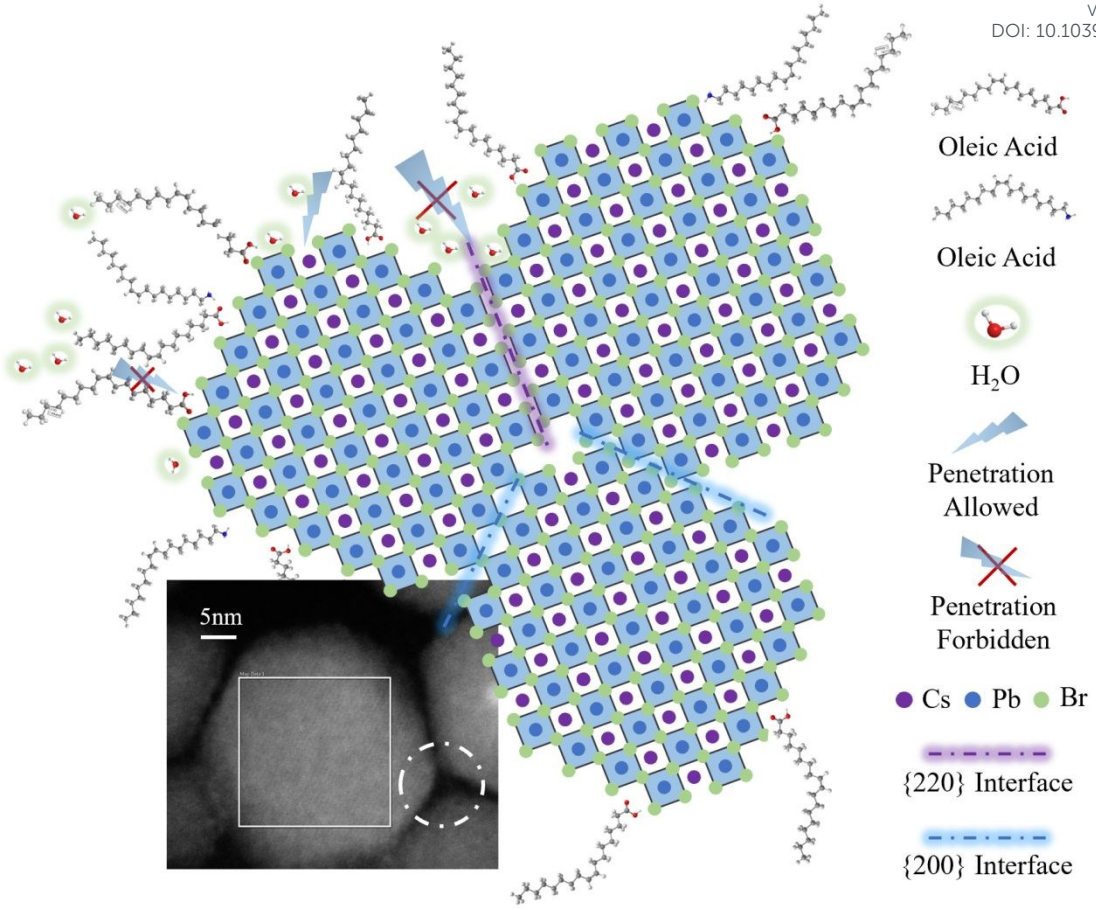

Fig. 5 The HAADF-STEM and diagram as the evidence of PeQD oriented attachment. The HAADF-STEM image exhibits the direct contact of three AcOEt-treated PeQDs with edge truncated morphology. The diagram shows the corresponding arrangement of these three PeQDs surrounding the white dotted circle in the HAADF-STEM image (the left one represents the centre PeQD marked with a white box). There are two different interfaces: {220} interface and {200} interface. It is shown that H_2O molecules have difficulty infiltrating into the {220} interface attributed to the contact between two facets in the {220} group.

Reference

1. L. Protesescu, S. Yakunin, M. I. Bodnarchuk, F. Krieg, R. Caputo, C. H. Hendon, R. X. Yang, A. Walsh and M. V. Kovalenko, *Nano letters*, 2015, **15**, 3692-3696.
2. H. C. Wang, Z. Bao, H. Y. Tsai, A. C. Tang and R. S. Liu, *Small*, 2018, **14**.
3. Y. Kim, E. Yassitepe, O. Voznyy, R. Comin, G. Walters, X. Gong, P. Kanjanaboos, A. F. Nogueira and E. H. Sargent, *ACS Appl Mater Interfaces*, 2015, **7**, 25007-25013.
4. J. Song, J. Li, X. Li, L. Xu, Y. Dong and H. Zeng, *Adv Mater*, 2015, **27**, 7162-7167.
5. Y. Chen, Y. Chu, X. Wu, W. Ou-Yang and J. Huang, *Adv Mater*, 2017, **29**.
6. B. Hou, *Israel Journal of Chemistry*, 2019, **59**, 637-638.
7. Y. Zhao, J. Li, Y. Dong and J. Song, *Israel Journal of Chemistry*, 2019, **59**, 649-660.
8. B. Li, M. Lu, J. Feng, J. Zhang, P. M. Smowton, J. I. Sohn, I.-K. Park, H. Zhong and B. Hou, *Journal of Materials Chemistry C*, 2020, 8, 10676-10695.
9. Y. Chen, Y. Chu, X. Wu, W. Ou-Yang and J. Huang, *Advanced Materials*, 2017, **29**, 1704062.
10. C. Zou, Y. Xi, C. Y. Huang, E. G. Keeler, T. Feng, S. Zhu, L. D. Pozzo and L. Y. Lin, *Advanced Optical Materials*, 2018, **6**.
11. D. K. Hwang, Y. T. Lee, H. S. Lee, Y. J. Lee, S. H. Shokouh, J.-h. Kyhm, J. Lee, H. H. Kim, T.-H. Yoo, S. H. Nam, D. I. Son, B.-K. Ju, M.-C. Park, J. D. Song, W. K. Choi and S. Im, *NPG Asia Materials*, 2016, **8**, e233-e233.
12. M. Chen, H. Lu, N. M. Abdelazim, Y. Zhu, Z. Wang, W. Ren, S. V. Kershaw, A. L. Rogach and N. Zhao, *ACS nano*, 2017, **11**, 5614-5622.
13. C. Y. Wu, Z. Wang, L. Liang, T. Gui, W. Zhong, R. C. Du, C. Xie, L. Wang and L. B. Luo, *Small*, 2019, **15**, 1900730.
14. Y. Yang, H. Dai, F. Yang, Y. Zhang, D. Luo, X. Zhang, K. Wang, X. W. Sun and J. Yao, *Nanoscale research letters*, 2019, **14**, 1-8.
15. F. Li, C. Ma, H. Wang, W. Hu, W. Yu, A. D. Sheikh and T. Wu, *Nature communications*, 2015, **6**, 8238.
16. J. Z. Fan, N. T. Andersen, M. Biondi, P. Todorović, B. Sun, O. Ouellette, J. Abed, L. K. Sagar, M. J. Choi and S. Hoogland, *Advanced Materials*, 2019, **31**, 1904304.
17. J. Kim, S.-M. Kwon, Y. K. Kang, Y.-H. Kim, M.-J. Lee, K. Han, A. Facchetti, M.-G. Kim and S. K. Park, *Science Advances*, 2019, **5**, eaax8801.
18. J.-K. Sun, S. Huang, X.-Z. Liu, Q. Xu, Q.-H. Zhang, W.-J. Jiang, D.-J. Xue, J.-C. Xu, J.-Y. Ma and J. Ding, *Journal of the American Chemical Society*, 2018, **140**, 11705-11715.
19. N. Soetan, W. R. Erwin, A. M. Tonigan, D. G. Walker and R. Bardhan, *The Journal of Physical Chemistry C*, 2017, **121**, 18186-18194.
20. L. Wang, B. Liu, X. Zhao, H. V. Demir, H. Gu and H. Sun, *ACS applied materials & interfaces*, 2018, **10**, 19828-19835.
21. T. Chiba, K. Hoshi, Y. J. Pu, Y. Takeda, Y. Hayashi, S. Ohisa, S. Kawata and J. Kido, *ACS Appl Mater Interfaces*, 2017, **9**, 18054-18060.
22. L. Zhou, K. Yu, F. Yang, H. Cong, N. Wang, J. Zheng, Y. Zuo, C. Li, B. Cheng and Q. Wang, *Journal of Materials Chemistry C*, 2017, **5**, 6224-6233.
23. K. Hoshi, T. Chiba, J. Sato, Y. Hayashi, Y. Takahashi, H. Ebe, S. Ohisa and J. Kido, *ACS applied materials & interfaces*, 2018, **10**, 24607-24612.
24. M. Leng, Y. Yang, K. Zeng, Z. Chen, Z. Tan, S. Li, J. Li, B. Xu, D. Li and M. P. Hautzinger, *Advanced Functional Materials*, 2018, **28**, 1704446.
25. S. Wang, C. Bi, J. Yuan, L. Zhang and J. Tian, *ACS Energy Letters*, 2017, **3**, 245-251.
26. H. Yang, Y. Feng, Z. Tu, K. Su, X. Fan, B. Liu, Z. Shi, Y. Zhang, C. Zhao and B. Zhang, *Nano Research*, 2019, **12**, 3129-3134.
27. X. Li, Y. Wu, S. Zhang, B. Cai, Y. Gu, J. Song and H. Zeng, *Advanced Functional Materials*, 2016, **26**, 2435-2445.
28. S. Zhan, S. Han, S. Y. Bang, B. Li, Y. T. Chun, B. Hou and J. M. Kim, *physica status solidi (a)*.

29. T. Chiba, Y. Hayashi, H. Ebe, K. Hoshi, J. Sato, S. Sato, Y.-J. Pu, S. Ohisa and J. Kido, *Nature Photonics*, 2018, **12**, 681-687.
30. Y. Zhai, X. Bai, G. Pan, J. Zhu, H. Shao, B. Dong, L. Xu and H. Song, *Nanoscale*, 2019, **11**, 2484-2491.
31. H. Wu, H. Si, Z. Zhang, Z. Kang, P. Wu, L. Zhou, S. Zhang, Z. Zhang, Q. Liao and Y. Zhang, *Adv Sci (Weinh)*, 2018, **5**, 1801219.
32. Y. Li, X. Hou, X. Dai, Z. Yao, L. Lv, Y. Jin and X. Peng, *J Am Chem Soc*, 2019, **141**, 6448-6452.
33. Y.-H. Suh, T. Kim, J. W. Choi, C.-L. Lee and J. Park, *ACS Applied Nano Materials*, 2018, **1**, 488-496.
34. Y. H. Kim, H. Cho, J. H. Heo, T. S. Kim, N. Myoung, C. L. Lee, S. H. Im and T. W. Lee, *Advanced materials*, 2015, **27**, 1248-1254.
35. Z. K. Tan, R. S. Moghaddam, M. L. Lai, P. Docampo, R. Higler, F. Deschler, M. Price, A. Sadhanala, L. M. Pazos, D. Credgington, F. Hanusch, T. Bein, H. J. Snaith and R. H. Friend, *Nature Nanotechnology*, 2014, **9**, 687-692.
36. H. Cho, S.-H. Jeong, M.-H. Park, Y.-H. Kim, C. Wolf, C.-L. Lee, J. H. Heo, A. Sadhanala, N. Myoung and S. Yoo, *Science*, 2015, **350**, 1222-1225.
37. E. Mosconi, J. M. Azpiroz and F. De Angelis, *Chemistry of Materials*, 2015, **27**, 4885-4892.
38. F. Bertolotti, L. Protesescu, M. V. Kovalenko, S. Yakunin, A. Cervellino, S. J. Billinge, M. W. Terban, J. S. Pedersen, N. Masciocchi and A. Guagliardi, *ACS nano*, 2017, **11**, 3819-3831.
39. N. Kattan, B. Hou, D. J. Fermín and D. Cherns, *Applied Materials Today*, 2015, **1**, 52-59.
40. L. Sun, J. J. Choi, D. Stachnik, A. C. Bartnik, B. R. Hyun, G. G. Malliaras, T. Hanrath and F. W. Wise, *Nature Nanotechnology*, 2012, **7**, 369-373.